Local rheological probes for complex fluids: Application to Laponite suspensions

C. Wilhelm,[1,2] F. Elias,[1,2,*] J. Browaeys,[2,3] A. Ponton,[2,3] and J.-C. Bacri[1,2]
[1]*Laboratoire des Milieux Désordonnés et Hétérogènes, Université Paris 6, Tour 13, Case 78, 4 place Jussieu, 75252 Paris Cedex 05, France*
[2]*Fédération de Recherche FR 2438 "Matiére et Systémes Complexes," Paris, France*
[3]*Laboratoire de Biorhéologie et d'Hydrodynamique Physico-Chimique, Université Paris 7, Tour 33-34, Case 7056, 2 place Jussieu, 75251 Paris Cedex 05, France*
(Received 21 March 2002; published 19 August 2002)

We present an experimental method allowing a direct measurement of the local rheological behavior of complex fluids. A magnetic probe is inserted into the bulk of the fluid and submitted to a controlled magnetic force or torque, which induces a mechanical perturbation of the fluid. The geometry of the perturbation can be varied using two kinds of probes: a magnetic bead submitted to a homogeneous magnetic force in one direction, and a magnetic needle that can turn inside the material under the effect of an applied magnetic torque. Two complex viscoelastic fluids are investigated. First, a surfactant solution, which has a linear mechanical behavior in the range of the applied stresses, is used to test and validate the experimental methodology. We then use the local probes to investigate a Laponite colloidal suspension, which exhibits nonlinear behavior such as thixotropy, shear thinning, and aging. In this latter fluid, we find an exponential growth of the rheological relaxation time versus the system age, a power-law dependence of the fluid viscosity on the applied stress, and a dynamical yield stress which saturates with the fluid aging time.

DOI: 10.1103/PhysRevE.66.021502 PACS number(s): 83.60.Bc, 61.20.Lc

I. INTRODUCTION

Complex fluids such as colloids, emulsions, foams, polymer or surfactant solutions are multiphasic materials [1]. Their constitutive entities are in interaction; the competition between the different energies generates structures at many different length scales in the fluid. This results in a diversity of the fluid macroscopic rheological behavior, which can vary as a function of time (aging [2]), or as a function of the applied stress (elastic-plastic transition [3], shear thinning, shear thickening, thixotropy [4]).

The rheology of these soft materials has been the subject of many investigations. Experimentally, several methods are frequently used. Classical rheometry consists of globally shearing (stressing) the sample between two plates and recording the stress (strain) applied by the sample onto the shearing plate [5]. This allows the geometry and the frequency of the shear to be varied and is a very powerful technique to investigate materials with a linear response. However, in the case of nonlinear materials, the deformation field inside the sample does not decrease linearly with increasing distance from the shearing plate. Models based on an inhomogeneous strain distribution inside the stressed fluid accurately account for the nonlinearities of the macroscopic stress-strain curve [3,6]. Nevertheless, the results obtained by using standard rheological measurement do not directly account for such heterogeneities. Dynamic light scattering and diffusive wave spectroscopy involve measuring the correlation function of the positions inside the material. These methods can be either nonintrusive if the objects followed are constitutive of the studied material [7–11], or intrusive if tracer particles are added to the material [7,11]. In order to link the observed diffusive motion of the followed objects to the internal mechanics of the material, microscopic mechanical models have been formulated [7,11,12]. However, in the case of nonequilibrium systems presenting an aging behavior, no obvious relation exists in theory [13] although such a link is experimentally observed and thus empirically assumed.

Recently, direct microscopic rheological measurements have been developed in the domain of biophysics, to investigate the micromechanics of complex biological systems (network of actin filaments, or living cells) on the scale of its constituents [14–17]. A microscopic magnetic bead is inserted into the material to be investigated and submitted to a controlled magnetic force. The bead displacement in response to the external perturbation then gives access to the measurement of the local viscoelastic moduli. An alternative method, based on the rotation of colloidal magnetic probes, is also commonly used to measure the local viscosity of fluids at the nanoscopic scale [18].

In this paper, we generalize these experimental methods to allow the systematic direct investigation of the local rheology of complex fluids. Two tools are developed, based on the translation or rotation of a magnetic probe inside the fluid to be investigated under the effect of an applied magnetic force or torque, which equilibrates with the elastic and viscous forces or torques applied by the fluid to the probe. Using an appropriate model for the viscoelastic behavior of the fluid, the equation of motion of the probe is deduced. An analysis of the probe displacement allows the fluid elastic and viscous moduli to be measured. We use two types of magnetic probes inserted in the bulk of the material: a paramagnetic spherical bead submitted to a constant magnetic force which adopts a translation motion in the material, and a

*Corresponding author. Email address: elias@ccr.jussieu.fr

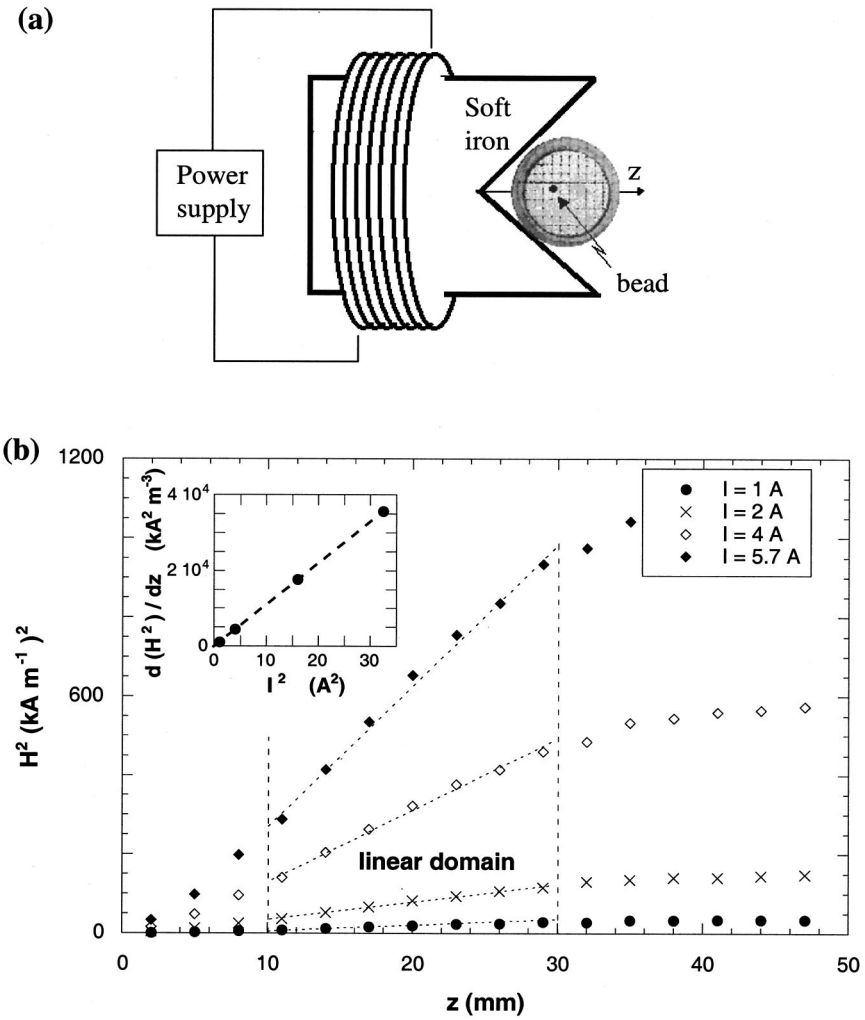

FIG. 1. (a) Top view of the experimental setup used in order to induce a linear displacement of a magnetic steel bead inside a complex fluid under the effect of a magnetic force. The fluid is placed in a closed cylindrical chamber of 1 cm diameter and 1 cm height and the magnetic bead (radius $R=0.5$ mm) is inserted in the bulk. Two pieces of soft iron inside a coil generate a homogeneous gradient of H^2 (H being the amplitude of the external magnetic field) in the z horizontal direction. Therefore, a homogeneous magnetic force is applied on the paramagnetic bead. The underlying grid on the image is a millimetric grid. (b) Plot of H^2 as a function of the distance to the center of the polar pieces in the z direction for different intensities I of the electric current in the coil: the gradient of H^2 is constant for 1 cm$<z<$3 cm. Inset, variation of ∇H^2 vs I in the region 1 cm$<z<$3 cm.

ferromagnetic needle submitted to a magnetic torque, which rotates in the fluid. These two probes allow the geometry of the perturbation to be varied.

The paper is organized as follows. The experimental setup is presented in Sec. II. The experimental methodology is then validated using a linear viscoelastic fluid (Sec. III), comparing the fluid rheological characteristics determined using the two types of local probes to measurements performed using a standard rheometer. In Sec. IV, local probes are used to describe the local rheology of a complex colloidal glass, a Laponite suspension. The aging behavior, shear thinning, and thixotropy of this fluid are investigated. The results obtained and the further applications of this technique are discussed in Sec. V. Because the probes are macroscopic (their typical size is 1 mm), the results are not at this stage qualitatively different from the results that can be obtained using standard rheometry. However, the fluid is investigated at a local scale. A promising application of the experimental method presented here is the variation of the rotating probe size from millimetric to nanoscopic, in order to probe, by the means of rheology, all the different pertinent length scales of the fluid. Another possible application is the determination of the viscoelastic properties of anisotropic materials.

II. EXPERIMENTAL SETUP

A. Translation of a paramagnetic bead

This technique is based on the linear translation of a magnetic spherical bead in the fluid under the effect of a controlled homogeneous magnetic force. The bead, made of steel, has a radius $R=0.5$ mm. The measurement of the bead magnetization as a function of an applied magnetic field, performed using a Foner device [19], shows that the bead has a paramagnetic behavior. For the magnetic field amplitudes used in the experiments, the bead volume magnetization $\boldsymbol{M_B}$ increases linearly with the applied magnetic field $\boldsymbol{H}$: $\boldsymbol{M_B}=\chi\boldsymbol{H}$, where χ is the bead magnetic susceptibility.

Inside the complex fluid to be investigated, the bead is submitted to a magnetic force $\boldsymbol{F}$ generated by the gradient of the magnetic field $\boldsymbol{H}$,

$$\boldsymbol{F}=\mu_0 V_B(\boldsymbol{M_B}\cdot\boldsymbol{\nabla})\boldsymbol{H}=\tfrac{1}{2}\mu_0 V_B\chi\boldsymbol{\nabla}(H^2), \qquad (1)$$

where V_B is the bead volume. To ensure that $\boldsymbol{F}$ is constant along the bead displacement, a homogeneous gradient of H^2 is generated using two pieces of soft iron placed inside a coil in the configuration illustrated in Fig. 1(a). The variation of H^2 along the horizontal z axis is presented in Fig. 1(b): it

remains linear over a 2 cm wide region. In this region, the external magnetic force is along the z axis and the amplitude of the force can be controlled by varying the intensity of the electric current in the coil.

A cylindrical sealed chamber of 1 cm diameter and 1 cm height is filled with the fluid to be investigated. The magnetic bead is inserted in the bulk of the fluid by using a magnet. When the magnetic field is applied, the bead moves along the direction of the z axis. The coil is driven by an alternating square wave form electric current, therefore the relaxation of the bead motion with or without the applied magnetic force can be analyzed. The bead displacement is followed using a charge-coupled device camera placed above the chamber, the images are digitized by the frame grabber of a computer, and the space-time diagrams are recorded in order to obtain the bead displacement z versus time t.

To calibrate the magnetic force using Eq. (1), the bead magnetic susceptibility has to be determined. This is achieved by placing the setup with the z axis pointing upwards, with the chamber filled with glycerol, a Newtonian viscous fluid. In the absence of an applied magnetic force, the bead falls due to its own weight P_B, with a constant velocity $u_1 = P_B/(6\pi\eta R)$ where η is the glycerol viscosity and $P_B = \Delta\rho V_B g$, with $\Delta\rho$ the density difference between steel and glycerol (Stokes experiment).[1] When a magnetic force $\boldsymbol{F}$ is applied, the bead moves upwards with a constant velocity $u_2 = (F - P_B)/(6\pi\eta R)$. This allows to check the homogeneity of the applied magnetic force along the z axis. Using Eq. (1), the bead magnetic susceptibility is

$$\chi = \frac{2P_B}{V_B \mu_0 \boldsymbol{\nabla}(H^2)} \left(1 - \frac{u_2}{u_1}\right).$$

Using a bead of radius $R = 0.5$ mm, we determine the magnetic susceptibility of the steel bead to be $\chi = 3.9$.[2]

In the subsequent experiments (Secs. III and IV), the contribution of gravity is suppressed by placing the z axis in the horizontal position, so that the magnetic force is the only external force to be considered for the horizontal bead displacement. Setting the intensity of the electric current in the coil at a fixed value between 0 and 6 A, the amplitude of the applied magnetic force can be adjusted between 0 and 50 μN.

[1]The Reynolds number is small enough to ensure a Stokes flow: $\mathrm{Re} \approx uR/v \approx 10^{-2}$, where v is the fluid dynamic viscosity.

[2]This value of χ corresponds to an effective magnetic susceptibility for the steel bead, which is due to its shape. For a finite object, the effective susceptibility is $\chi = \chi_{\mathrm{bulk}}/(1 + \chi_{\mathrm{bulk}} D)$, where χ_{bulk} is the magnetic susceptibility of the bulk material and D is the demagnetizing factor, due to the magnetic dipolar interactions inside the object. D strongly depends on the object shape: $D = 1/3$ for a spherical monodomain bead. As $\chi_{\mathrm{bulk}} \approx 10^3 \gg 1/D$ for steel, the effective susceptibility of the steel bead is $\chi \cong 1/D \cong 3$, which is of the order of magnitude of the measured value (the discrepancy probably comes from the bead not being perfectly monodomain, thus $D < 1/3$).

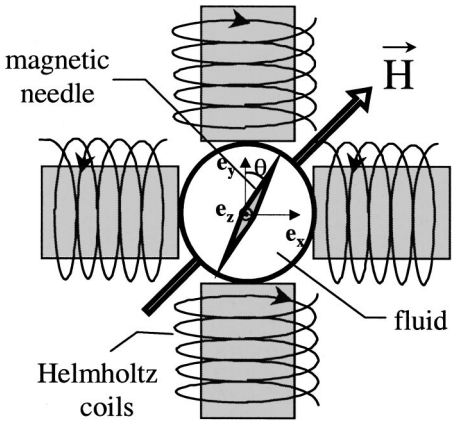

FIG. 2. Experimental setup used in order to induce a rotation of a cylindrical magnetic nickel needle inside a complex fluid. The needle is 650 μm long and 50 μm in diameter. The complex fluid is placed in the same cylindrical chamber as in Fig. 1(a) and the magnetic needle is inserted in the bulk. Two pairs of coils in the Helmholtz configuration provide a magnetic field whose direction can be adjusted. The applied magnetic field used in the experiments is either rotating if the two pairs of coils are supplied with an alternating current 90° out of phase, or static making an angle of $\beta = 45°$ with the needle initial orientation as sketched here.

B. Rotation of a ferromagnetic needle

For this technique, a cylindrical ferromagnetic needle is made to rotate in the bulk of the studied fluid under the influence of a controlled magnetic torque. The needle, made of nickel, has a diameter of 50 μm and a length of 650 μm. We assume the volume magnetization of the Nickel needle to be the same as the bulk volume magnetization $M_N = 4.85 \times 10^5$ A m^{-1}, since demagnetizing effects are negligible for such a geometry. $\boldsymbol{M_N}$ is aligned along the long axis of the needle. Using the experimental setup illustrated in Fig. 2, a magnetic torque is applied to the needle by means of a static magnetic field whose direction makes an angle β with respect to the initial orientation of the needle. If one defines θ, the angle through which the needle has turned with respect to its initial orientation along the y axis, the magnetic torque exerted on the needle can be written,

$$\boldsymbol{\Gamma} = \mu_0 V_N \boldsymbol{M_N} \times \boldsymbol{H} = \boldsymbol{\Gamma_0} \sin(\beta - \theta), \tag{2}$$

where V_N is the needle volume and $\boldsymbol{\Gamma_0} = \mu_0 V_N M_N H \boldsymbol{e_z}$. The initial torque is $\boldsymbol{\Gamma_i}(H, \beta) = \boldsymbol{\Gamma_0}(H) \sin\beta$. In the following, β is fixed to 45° and H is the system control parameter. For the magnetic field amplitudes used in the experiment ($0 < H < 6$ kA m^{-1}), Γ_0 can be varied between 0 and 4×10^{-9} J.

A cylindrical sealed chamber of 1 cm diameter and 1 cm height, filled with the fluid to be investigated and containing the needle is placed under a microscope, and the rotation of the needle towards the static magnetic field direction is followed using video imaging as previously described. The space-time diagrams give plots of the needle rotation θ as a function of time. Measurements in glycerol cannot be performed because of the sedimentation of the needle which occurs too rapidly to allow a precise measurement.

Equations (1) and (2) give the magnetic force applied to the bead and the magnetic torque applied to the needle as a function of the control parameters. When the probe is inserted in the fluid under investigation, this force (torque) equilibrates with the fluid viscous and elastic forces (torques) applied to the bead (needle), which can therefore be measured.

III. VALIDATION USING A LINEAR VISCOELASTIC FLUID

In this section, a fluid having a linear Maxwellian rheological behavior is investigated. Three different experimental methods are used to measure the viscoelastic characteristics of the fluid: a standard Couette rheometer, a magnetic bead inserted in the fluid and submitted to a magnetic force, and a magnetic needle submitted to a magnetic torque inside the fluid. Each method shows that the rheological behavior of the fluid is Maxwellian in the range of the applied stress. The numerical values of the fluid viscous and elastic moduli determined independently in each method are identical within experimental errors. This validates the experimental methodology based on the use of the two local rheological probes.

A. Sample description

It is well known that surfactant molecules in aqueous solutions can form long elongated wormlike micelles above the critical micellar concentration [3,20]. The micellar growth is controlled by several parameters such as surfactant concentration or the addition of a salt. The equilibrium static and dynamic properties of these locally cylindrical surfactant assemblies depart from those of a polymer solution whose dynamics is described by the reptation model (characteristic time τ_{rep}) in the sense that flexible wormlike micelles can break and recombine reversibly with a characteristic time τ_{break}.

A specific model [21] has been developed to describe the dynamical properties of these systems. In the regime when scission reactions are rapid on the time scale of reptation ($\tau_{\mathrm{break}} < \tau_{\mathrm{rep}}$) the stress relaxation is a single exponential. Solutions of surfactant are then good examples of well characterized viscoelastic fluids, exhibiting a Maxwellian behavior.

The system chosen for this study is composed of the cationic surfactant cethyltrimethylammonium choride (CTAC) in distilled water and an additive salt (sodium salicylate, NaSal) which favors the formation of micelles. The molar concentrations are, respectively, $[\mathrm{CTAC}] = 0.1$ M and $[\mathrm{NaSal}] = 0.17$ M.

B. Standard rheology

We initially characterize this system using a standard Couette rheometer fitted with a cone and plate device (4 cm diameter, 2° angle). From oscillatory shear measurements the linear viscoelastic domain is first determined by a stress sweep (0.5–25 Pa) at a constant angular frequency ($\omega = 6.3\ \mathrm{rad\,s^{-1}}$). The storage G' and loss G'' moduli are then measured by an angular frequency sweep in the range between 0.063 and 63 $\mathrm{rad\,s^{-1}}$.

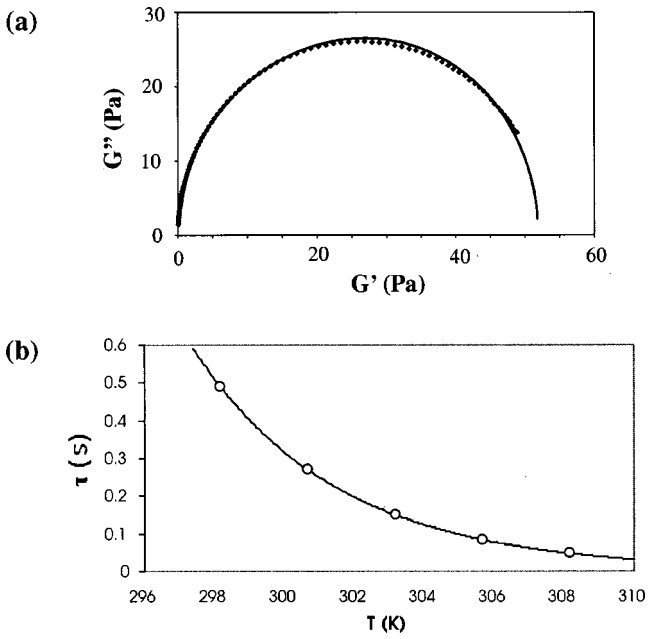

FIG. 3. (a) Cole Cole plot for an aqueous solution of [CATC] = 0.1 M and [NaSal] = 0.17 M at $T = 25\,^{\circ}\mathrm{C}$. The solid line is the fit obtained using the Maxwell model [Eq. (3)]. (b) Plot of the rheological characteristic time τ_R vs the temperature T. The solid line is the fit obtained using Eq. (5).

In the case of a Maxwell fluid (single relaxation time), the angular frequency dependence of G' and G'' are given by

$$G' = \frac{G\omega^2\tau_R^2}{1+\omega^2\tau_R^2}, \quad G'' = \frac{G\omega\tau_R}{1+\omega^2\tau_R^2}, \tag{3}$$

where the relaxation time τ_R is defined as the ratio of viscosity η and shear modulus G,

$$\tau_R = \frac{\eta}{G}. \tag{4}$$

The linear representation of G'' versus G' is a semicircle (Cole Cole plot) which is characteristic of a Maxwell behavior. Figure 3(a) presents the Cole Cole plot for the investigated surfactant sample at $T = 25\,^{\circ}\mathrm{C}$. The solid line, which represents the predictions of the Maxwell model [Eq. (3)], is in good agreement with the experimental results. Such an analysis gives $G(25\,^{\circ}\mathrm{C}) = (48 \pm 9)$ Pa and $\tau_R(25\,^{\circ}\mathrm{C}) = (0.49 \pm 0.10)$ s; the error is mainly due to the experiments not being perfectly reproducible. With increasing temperature, the shear modulus G remains constant within error. An equation of the Williams-Landel-Ferry form is appropriate to describe the evolution of the relaxation time with temperature [22],

$$\tau_R[T(\mathrm{K})] = \tau_0 \exp\left(\frac{-C_1(T-T_0)}{C_2+T-T_0}\right), \tag{5}$$

with $\tau_0 = 0.51$ s, $T_0 = 298$ K, $C_1 = 79.4$ K, and $C_2 = 328.6$ K. Figure 3(b) represents the variation of τ_R versus T, fitted by Eq. (5).

C. Local rheology

The insertion of a local probe in motion within the fluid allows to determine the viscous and elastic moduli of the fluid. Using appropriate Maxwell mechanical equivalent circuits, the equation of motion of the probe inside the fluid is obtained as a function of the external magnetic force [Eq. (1)] or torque [Eq. (2)] applied to the probe. The shear modulus and the viscosity of the fluid are then deduced from a fit of the probe motion, and compared to the results obtained in Sec. III B.

1. Translating bead

The paramagnetic bead inside the fluid is submitted to a homogeneous magnetic force F, at a measured temperature $T=30\,^{\circ}\mathrm{C}$. The appropriate Maxwell mechanical equivalent circuit consists of a spring of elastic constant k (return elastic force $-kz$) and a dashpot of viscous constant γ (drag force $-\gamma\dot{z}$) in series [Fig. 4(a)]; the equation of motion of the bead is then

$$\frac{\dot{F}}{k}+\frac{F}{\gamma}=\dot{z}. \tag{6}$$

For a step force F_0 applied at $t=0$, the solution of the Maxwell model can be written

$$z(t)=\frac{F_0}{k}+\frac{F_0}{\gamma}t. \tag{7}$$

A typical bead displacement $z(t)$ is shown in Fig. 4(b). The parameters F_0/k and F_0/γ are determined for five different applied forces using Eq. (7) to fit experimental curves. They are plotted in Fig. 4(c) as a function of the applied force F_0. They increase linearly with F_0 as expected for a Maxwellian fluid. At $T=30\,^{\circ}\mathrm{C}$, one obtains $k=(0.42\pm0.04)$ Pa m and $\gamma=(0.062\pm0.006)$ Pa s m. The experimental error is due to the slight discrepancies between independent experiments.

To compare these values with the results obtained in Sec. III B using a classical rheometer, the parameters γ and k must be linked to the viscosity η and the shear modulus G of the surrounding medium. On one hand, the drag force F_v exerted by a viscous medium on a spherical bead is given by the Stokes formula [23]: $F_v=-6\pi\eta R\dot{z}$ (the Reynolds number is very small: $\mathrm{Re}\cong 2\times10^{-4}$ at most), linking the parameter γ to the fluid viscosity η,

$$\gamma=6\pi\eta R, \tag{8}$$

where R is the bead radius. On the other hand, the displacement of a macroscopic bead embedded in an elastic medium is given in Ref. [24] by averaging the deformation generated by the elastic force F_e over the entire surface of the bead: $z=-(1/6\pi G)(F_e/R)$. The relation between the shear modulus G and the elastic parameter k is therefore given by[3]

$$k=6\pi GR. \tag{9}$$

This gives for the shear modulus $G=(45\pm4)$ Pa and the viscosity $\eta=(6.6\pm0.7)$ Pa s at $T=30\,^{\circ}\mathrm{C}$. At this temperature, measurements in a Couette rheometer (Sec. III B) give $G=(48\pm5)$ Pa and $\eta=(7.2\pm1.4)$ Pa s. The correct agreement between the different measurements validates our tech-

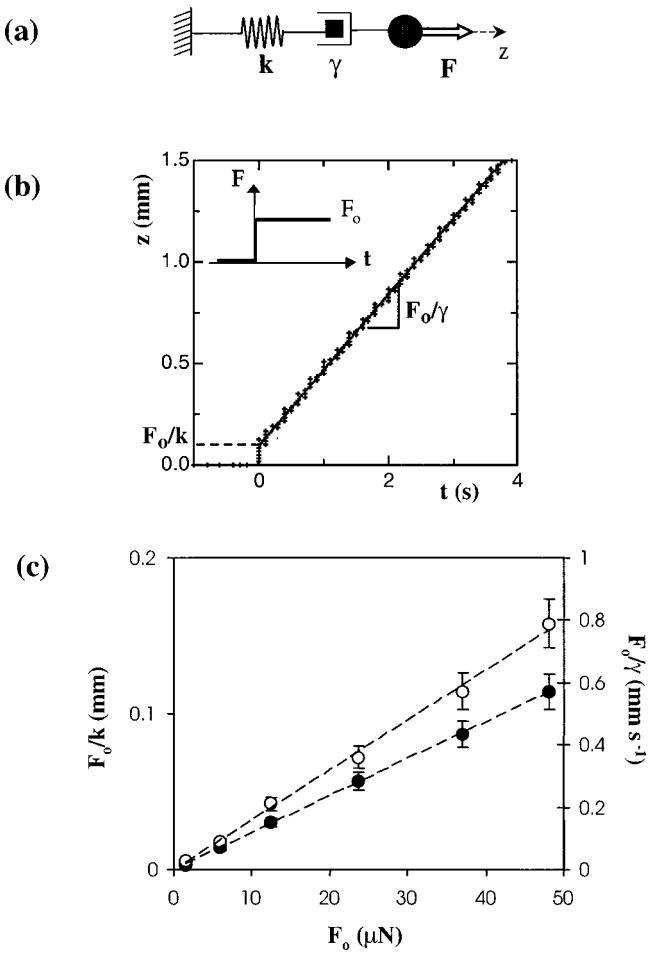

FIG. 4. (a) Maxwell mechanical equivalent circuit used to describe the displacement of the bead in the studied viscoelastic fluid, under the effect of an applied force. (b) Bead displacement in the Maxwellian fluid at $T=30\,^{\circ}\mathrm{C}$, under the effect of a homogeneous step force $F_0=26.7\ \mu$N applied to the bead at $t=0$. Solid line, best fit of the data using Eq. (3). (c) Variation of F_0/k (black dots) and F_0/γ (white dots) obtained from the fit shown in (b) as a function of the applied force strength F_0; k and γ do not depend on the applied force: $k=(0.42\pm0.04)$ Pa m and $\gamma=(0.062\pm0.006)$ Pa m s.

[3]Equation (9) is an equivalent of the Stokes equation [Eq. (8)] for an elastic medium. Let us notice that an equivalent generalization of the Stokes-Einstein equation is generally assumed in the case of microscopic particles submitted to Brownian motion inside a viscoelastic medium [7].

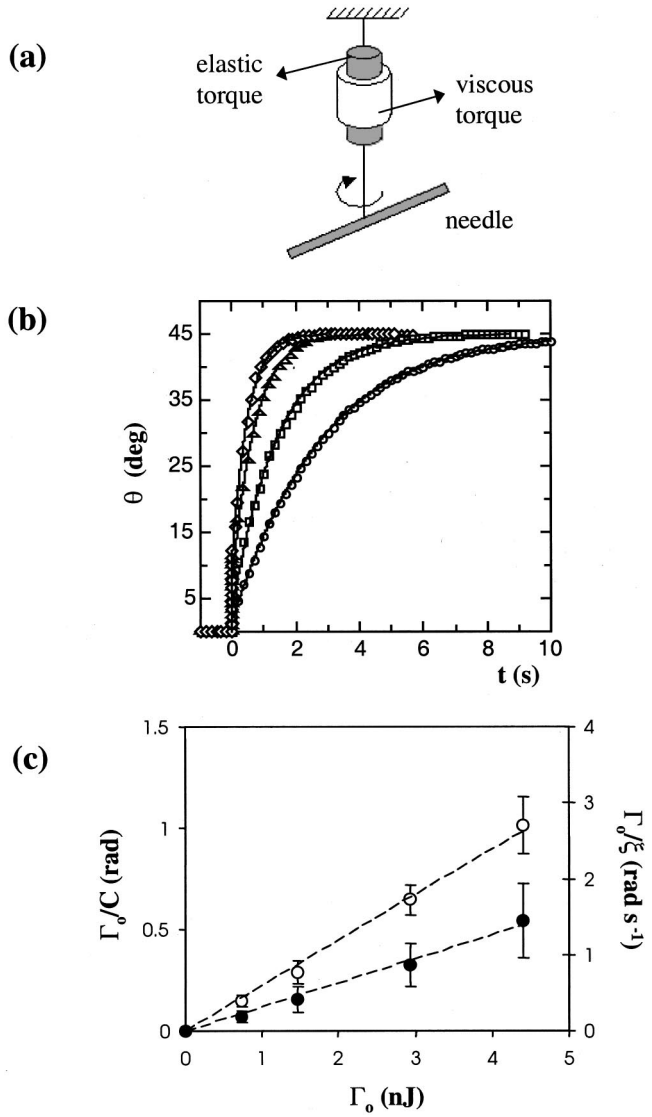

FIG. 5. (a) Maxwell mechanical equivalent circuit used to describe the needle rotation in the studied viscoelastic material, under the effect of an applied torque Γ. (b) Needle rotation in the Maxwell fluid under the effect of a step magnetic field H_0, applied at $t=0$ and making an angle of 45° with respect to the initial needle orientation. $T=29\,^{\circ}\mathrm{C}$. Different values of the magnetic torque Γ_0 are plotted. Solid line, best fit of the data using Eq. (9). (c) Variation of Γ_0/C (black dots) and Γ_0/ξ (white dots) obtained from the fit shown in (b) as a function of the applied initial torque Γ_0; C and ξ do not depend on the applied torque: $C=(9.2\pm1.7)\times10^{-9}$ Pa m^3 and $\xi=(1.76\pm0.15)\times10^{-9}$ Pa m^3 s.

nique for determining the viscoelastic linear parameters on a local macroscopic scale using a translating bead probe.

2. Rotating needle

The ferromagnetic needle inside the fluid is submitted to a magnetic torque Γ at a measured temperature $T=29\,^{\circ}\mathrm{C}$. In this geometry, we can model the system as a Maxwell mechanical equivalent circuit consisting of a dashpot coupled to a torsion wire, as represented in Fig. 5(a). The equation of motion of the needle can then be written as

$$\frac{\dot{\Gamma}}{C}+\frac{\Gamma}{\xi}=\dot{\theta}, \tag{10}$$

where Γ is the applied torque, θ is the angle through which the needle has turned, C is the wire elastic constant (return elastic torque $-C\theta$), and ξ is the dashpot viscous constant (drag torque $-\xi\dot{\theta}$). To test this hypothesis, we performed an experiment in which a ferromagnetic needle embedded in the Maxwellian micellar solution is submitted to a static magnetic field making an initial angle $\beta=45°$ with the initial needle orientation, as described in Sec. II B. A step magnetic field is applied: $H=0$ for $t<0$ and $H=H_0$ for $t\geqslant0$, resulting in the rotation of the needle towards the magnetic field direction. As the applied magnetic torque depends on the needle direction θ [Eq. (2)], calculations are required to derive from Eq. (10) the angle through which the needle has turned as a function of time. We define a new variable $\theta'=\beta-\theta$, and write

$$dt=-\left(\frac{\xi}{C}\cot\theta'+\frac{\xi}{\Gamma_0}\frac{1}{\sin\theta'}\right)$$

before integrating between 0^+ and t. One finally finds

$$t=\frac{\xi}{\Gamma_0}\ln\left|\frac{\tan\left(\frac{\beta-\theta_0}{2}\right)}{\tan\left(\frac{\beta-\theta}{2}\right)}\right|+\frac{\xi}{C}\ln\left|\frac{\sin(\beta-\theta_0)}{\sin(\beta-\theta)}\right|, \tag{11a}$$

where $\theta_0=\theta(0^+)$ is defined by

$$\theta_0=(\Gamma_0/C)\sin(\beta-\theta_0). \tag{11b}$$

Figure 5(b) shows a fit of the experimental data $\theta(t)$ using Eq. (9) with two fitting parameters: Γ_0/C and Γ_0/ξ. Again, the rheological behavior of the fluid is linear for the range of external torque used, as shown in Fig. 5(c). The measured viscoelastic parameters at $T=29\,^{\circ}\mathrm{C}$ (Sec. III B) are: $C=(9.2\pm1.7)\times10^{-9}$ Pa m^3 and $\xi=(1.8\pm0.1)\times10^{-9}$ Pa m^3 s. The errors here are due to the fit to the data using Eq. (9), which is larger than any error due to the reproducibility.

As in the case of the translating bead, the two parameters C and ξ must be linked to the fluid shear modulus and viscosity in order to be compared with the results obtained in Sec. III B using a classical rheometer. The relation between ξ and η is given in Ref. [25] for a cylinder of length L and diameter b,

$$\xi=\frac{\pi\eta L^3}{3\ln(L/2b)}. \tag{12}$$

This gives a local viscosity of $\eta=(11\pm1)$ Pa s, in good agreement with the value $\eta=(10\pm2)$ Pa s obtained with the Couette rheometer at $T=29\,^{\circ}\mathrm{C}$. This analysis validates *a posteriori* the proposed model described by Eq. (10). Moreover, the measured ratio $\xi/C=(0.20\pm0.05)$ s is close to the relaxation time $\tau_R=\eta/G=(0.19\pm0.04)$ s obtained with the Couette rheometer at $T=29\,^{\circ}\mathrm{C}$, reflecting that the elastic

parameter C is proportional to the shear modulus G with the same geometrical factor as the one linking the viscous parameter ξ to the viscosity η [Eq. (12)]. This is theoretically predicted [24] for a sphere rotating in a viscoelastic medium and seems to apply to the elongated shape considered here, so that the relation between the elastic constant C and the shear modulus G of the fluid can be written as

$$C=\frac{\pi G L^3}{3\ln(L/2b)}. \tag{13}$$

IV. APPLICATION TO THE LOCAL RHEOLOGY OF A LAPONITE SUSPENSION

Having validated the experimental methodology, both setups are used to explore the local rheology of Laponite, a complex colloidal fluid, which exhibits thixotropy, shear-thinning behavior, and glassy dynamics.

A. Sample description and preparation

Laponite is a synthetic clay ($Si_8Mg_{5.5}Li_{0.4}H_4O_{24}Na_{0.7}$) which consists of colloidal disklike particles of mean diameter 28 nm and thickness $\approx$1 nm [26,27]. The faces of the disks are charged negatively when the particles are suspended in an aqueous solution. The phase diagram of such Laponite suspension exhibits a liquid phase at low particle concentration, a viscoelastic isotropic phase and a viscoelastic birefringent nematic phase when the concentration is increased [28]. The structure of the isotropic viscoelastic phase, also called *pasty* phase, has been the subject of many studies and remains controversial. Whereas static and dynamic light scattering experiments initially revealed a fractal gel structure [29,30], Bonn *et al.* [31] have found no internal organization within the fluid. In fact, the structure of the pasty phase strongly depends on the suspension preparation and storage conditions [31,32]. The role of the ionic strength has also been invoked [33] to discriminate between two different regimes: a regime dominated by long-range electrostatic repulsion at low ionic strength ($<10^{-4}$ M) where the fluid adopts an amorphous structure, and a regime at high ionic strength where the electrostatic repulsion is screened and the particle anisotropy plays a role, giving an internal structure to the fluid [34]. Here, we are interested in the amorphous pasty phase of the Laponite suspension, obtained at low ionic strength. This phase slowly evolves in time, following a glassy dynamics [7,11,35]: its viscosity increases, and the relaxation times depend on the time at which the system has been prepared. A strong shaking can liquefy the fluid (thixotropy) and reset the aging time to zero: hence, this phenomenon is also called rejuvenation [36]. The liquid-paste transition of colloidal suspensions has therefore been described as a glass transition where the applied stress plays the role of temperature [37]: when the applied stress is decreased below a critical value (the yield stress), the system is quenched. Derec *et al.* [38] sketched a generic phase diagram for this transition in the stress–particle concentration space. The actual temperature does not seem to affect the Laponite suspension properties. In addition, the rheology of the suspension exhibits shear-thinning behavior: the viscosity decreases when the applied strain increases [39,40]. The variety of its mechanical behaviors makes this system a good model system for studying the rheology of complex materials.

The suspensions are prepared by dispersing Laponite particles at 2.7 wt % in distilled water under vigorous stirring at $p\mathrm{H}=10$ in order to avoid particle dissolution [41]. At this particle concentration, the solutions are in the pasty phase if no external shear is applied. The ionic strength is set at 10^{-4} M by adding NaOH to the water before dispersing the particles. Once prepared, the Laponite suspension is stored for 10 to 12 days in sealed vials under N_2 atmosphere in order to prevent dissolution of CO_2 from the air, which would lower the $p\mathrm{H}$ and affect the chemical stability of the suspension [32]. At $t=0$, the solution is filtered through a 0.8 μm microsept filtron, to break up eventual aggregates or structures [31]. Immediately after filtration, the suspension is placed in a 1 cm diameter chamber, a magnetic bead or needle is inserted, and the chamber is covered with a glass plate. This method allows to define a reproducible initial liquid state. After several minutes, the fluid becomes viscoelastic and the experiment can begin.

Let t_w be the time elapsed between the sample preparation in the chamber ($t=0$) and the application of the external mechanical perturbation. At $t'=t-t_w=0$, the probe inside the fluid is submitted to a step force or torque and its motion is analyzed. To perform a measurement, a mechanical perturbation is typically applied for several seconds, which is small compared to the fluid age t_w [limit of large Deborah number $\mathrm{De}=(\text{characteristic time})/(\text{time of experiment})=t_w/t' \gg 1$]. In this limit, a mechanical equivalent circuit can be used to describe the relaxation motion of the probe: the fluid viscous and elastic parameters deduced from this analysis do not depend on the duration of the measurement, although they depend on t_w. In the following, the displacement of the translating bead in the suspension is analyzed using a linear mechanical model presented in Sec. IV B. This model is used to investigate the influence of the system age on the viscoelastic parameters of the fluid (Sec. IV C), and the dependence of the fluid viscosity on the strength of the applied force (Sec. IV D). A needle in rotation in the Laponite suspension is then used (Sec. IV E) to analyze the effect of the magnetic torque applied to the needle on the elastic response of the fluid. In all the experiments presented here, the stress applied to the magnetic probes is of the order of 10 to 100 Pa (see Discussion). Such a mechanical perturbation modifies the rheological properties of the Laponite suspension. However, during its displacement, the magnetic bead or needle probes a region of the fluid which has not been previously sheared, although the fluid rheology has been modified behind the probe. We thus use the local magnetic probes both to perturb the fluid and to measure the modification of the viscoelastic parameters under the effect of the applied perturbation.

B. Mechanical linear model for the translating bead

At $t'=t-t_w=0$, the bead inside the fluid is submitted to a step force $F=F_0$. Its translation motion can be decom-

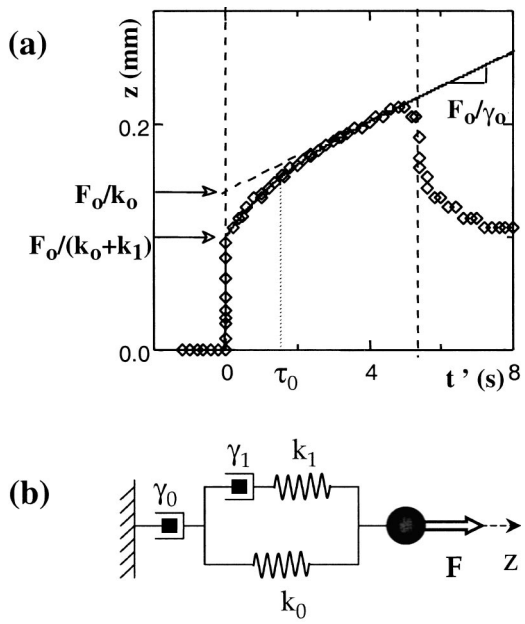

FIG. 6. (a) Bead displacement in a Laponite suspension under the effect of a step force $F_0=59.9\ \mu$N applied to the bead at $t=t_w=20$ min. Solid line, best fit of the data using Eq. (6), with four fitting parameters: k_0, k_1, γ_0, and γ_1. At $t'=t-t_w=5$ s, the force is set to zero and the magnetic bead moves backwards due to the fluid elasticity. (b) Kelvin-Voigt mechanical equivalent circuit used to describe the displacement of a bead in translation in the Laponite suspension.

posed into three regimes: an instantaneous elastic response at $t'=0$, a transient regime, and a viscous regime where the bead velocity is constant [Fig. 6(a)]. In order to deduce the fluid viscoelastic parameters, such a behavior can be described by a linear Kelvin-Voigt equivalent mechanical circuit involving four independent elastic and viscous parameters k_0, k_1, γ_0, and γ_1, as sketched in Fig. 6(b). In this model, the bead equation of motion is

$$\ddot{z}+\frac{1}{\tau_0}\dot{z}=\frac{1}{k_0+k_1}\ddot{F}+\left(\frac{1}{\gamma_0}+\frac{1}{k_0\tau_0}\right)\dot{F}+\frac{1}{\gamma_0\tau_0}F,$$

where

$$\tau_0=\frac{\gamma_1(k_0+k_1)}{k_0k_1}. \tag{14}$$

The solution of Eq. (13) for a step force F_0 applied at $t'=0$ is

$$\frac{z(t)}{F_0}=\frac{1}{k_0}\left\{1-\frac{k_1}{k_0+k_1}\exp\left(-\frac{t}{\tau}\right)\right\}+\frac{t}{\gamma_0}. \tag{15}$$

The four parameters k_0, k_1, γ_0, and γ_1 are obtained by fitting the experimental data $z(t)$ using Eq. (15). It is convenient to reduce the four independent parameters to two physical parameters: the sum $k=k_0+k_1$, representing the effective elastic parameter of the system at short times, and the viscous parameter γ_0, controlling the viscous regime at long times. An effective Maxwellian characteristic relaxation time can thus be defined as $\tau=\gamma_0/k=\gamma_0/(k_0+k_1)$.

C. Investigation of aging using the translating bead

The viscoelastic properties of the Laponite suspension are first investigated by varying t_w. Different cylindrical containers are filled with a Laponite suspension from the same preparation at $t=0$. The fluid evolves at rest in the container and a force is applied to the bead at $t=t_w$, during a time $t'=t-t_w\ll t_w$. Each experiment has been replicated a number of times in order to ensure reproducibility. Figure 7(a) shows the bead motion $z(t')$ for different aging times t_w. As t_w increases, the bead displacement slows down. This means that the viscoelastic moduli of the fluid increase: this behavior is characteristic of aging. In aging systems, the measured response of the system varies as a function of the system age in the following way: $z(t',t_w)=z[t'/a(t_w)]$, where $a(t_w)$ is an increasing function of t_w [42]. In the Laponite suspension investigated here, we observe an exponential growth of $a(t_w)$: $a(t_w)\approx\exp(t_w/\alpha)$, with $\alpha=(360\pm30)$ s$=(6.0\pm0.5)$ min [Fig. 7(b)]. Within the error bars, α does not depend on the strength of the applied force.

As the system does not have time to age during a single measurement, the fluid viscoelastic moduli can be determined using Eq. (15). The aging dynamics are then described by the evolution of the viscoelastic moduli with t_w. The four independent viscous and elastic parameters increase with t_w [Fig. 7(c)]. The effective Maxwellian characteristic relaxation time $\tau(t_w)$ grows exponentially with t_w: $\tau(t_w)\approx\exp(t_w/\beta)$ with $\beta=(710\pm50)$ s$=(12\pm1)$ min of the same order of magnitude as α.

D. Investigation of shear-thinning behavior using the translating bead

The rheological properties of the Laponite suspension have also been studied as a function of the strength of the force applied to the magnetic bead. The experimental procedure is presented in Fig. 8(a): at $t=t_w=t_1$, a step force of strength F_1 is applied to the bead and the relaxation motion of the bead is recorded. Subsequently, the force is released and the bead moves slightly backwards because of the fluid elasticity. At $t=t_2$, a second step force of amplitude F_2 is applied to the bead. The force is then released before a third step force of amplitude F_3 is applied at $t=t_3$, etc. The fluid viscoelastic moduli are measured as a function of the force amplitude using a linear analysis of the bead displacement under each perturbation. The total measuring time for this sequence is chosen to be small in comparison to the aging time t_w. This procedure allows a reliable comparison between the results obtained for different force amplitudes because the measurements are performed in the same chamber, which avoids problems of reproducibility due to the use of different containers. However, because of the small backwards motion of the bead when the force is released, the initial region in which the bead moves when a force is applied at the next step has already been sheared, and the fluid is softer in this region because of the shear-thinning effect. Therefore only the viscous regime of the bead displacement

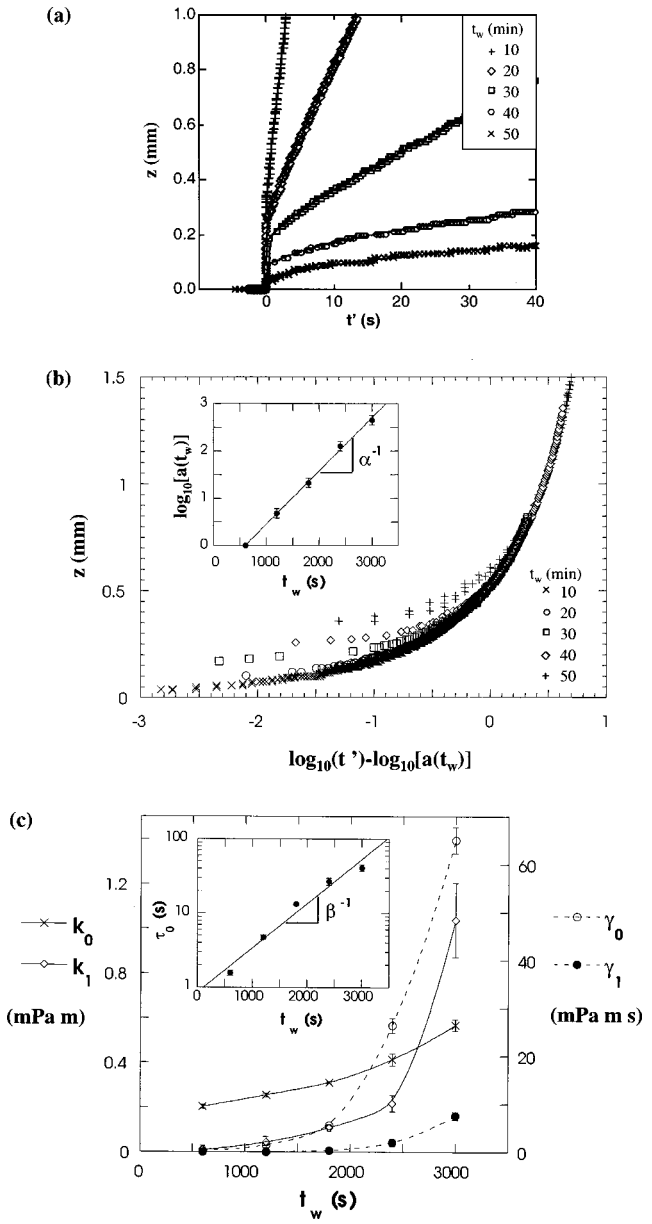

FIG. 7. (a) Bead displacement in a Laponite suspension for different aging times. After preparation, the suspension ages at rest for a time t_w. At $t'=t-t_w=0$, a constant force $F_0=37.0\ \mu$N is applied to the bead. When t_w increases, both the initial jump and the long-time slope of $z(t')$ decrease. This means that the viscous and the elastic moduli of Laponite suspension increase with increase in t_w. (b) Master curve obtained for the same aging times t_w as in (a), after translating horizontally all the curves $z[\log_{10}(t')]$ from a quantity $\log_{10}[a(t_w)]$, as suggested in Ref. [42]. The inset shows the variation of a vs t_w. The best fit of $a(t_w)$ is exponential: $a(t_w)\approx\exp(t_w/\alpha)$ with $\alpha=(360\pm30)$ s$=(6.0\pm0.5)$ min. (c) Evolution of the four linear viscoelastic parameters of the model presented in Fig. 6 as a function of t_w. All these parameters are increasing functions of t_w. Inset, time evolution of the effective Maxwelian relaxation time $\tau_0=\gamma_0/(k_0+k_1)$. Solid line, exponential fit of $\tau_0(t_w)$: $\tau_0(t_w)\approx\exp(t_w/\beta)$ with $\beta=(710\pm50)$ s$=(12\pm1)$ min of the same order of magnitude as α.

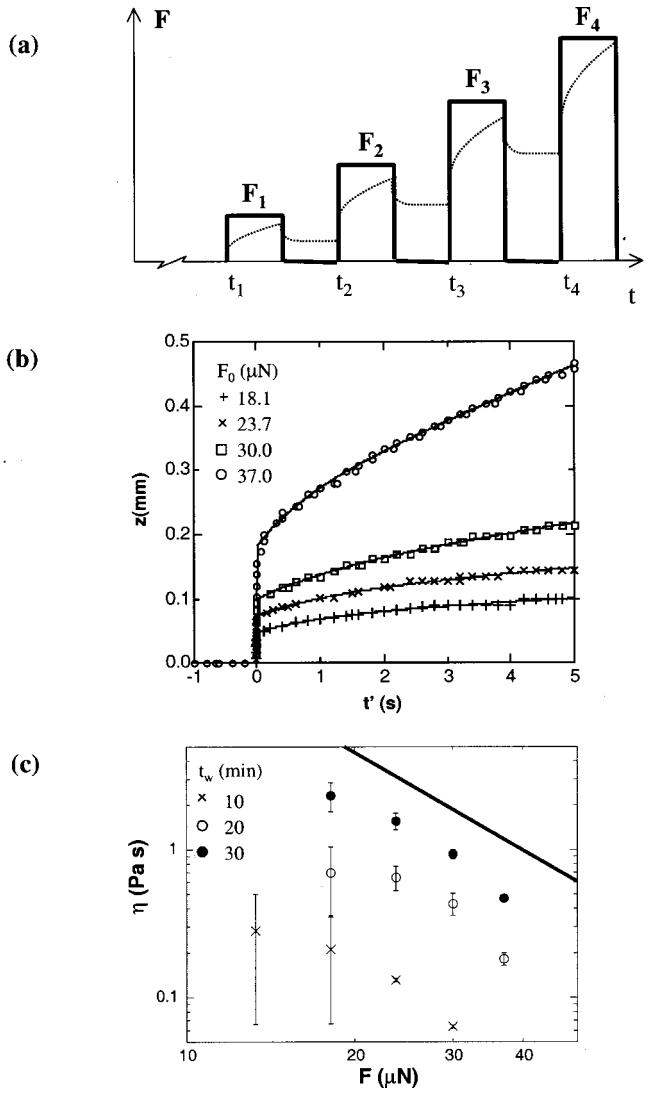

FIG. 8. (a) Sketch of the experimental procedure used to investigate the shear-thinning behavior of Laponite suspension. At $t=t_w$, the force is applied to the bead by steps of increasing amplitude. After each step the force is set to zero for the bead position to relax. The time between two steps is small compared to the aging time t_w of the suspension. The bead displacement is sketched in dotted lines. (b) Bead displacement in a Laponite suspension as a function of time for aging time $t_w=20$ min. Five different constant forces F are applied to the bead. (c) Viscosity of the Laponite suspension $\eta=\gamma_0/(6\pi R)$ in the viscous regime of the bead displacement as a function of the applied force strength F, for different aging times. The solid line represents a power-law variation $\eta\approx F^{-\delta}$ with $\delta=2$.

can be analyzed, since it is only in this regime that the bead explores a region which has not previously been sheared. Figure 8(b) shows the bead motion $z(t')$ for different applied forces. Figure 8(c) represents the variation of the fluid viscosity $\eta=\gamma_0/(6\pi R)$ [Eq. (8)] as a function of the applied force F, for different aging times. η is a decreasing function of F, which is characteristic of the shear-thinning behavior of Laponite suspensions. Within error bars, the variation of η versus F is compatible with a power-law behavior. We find

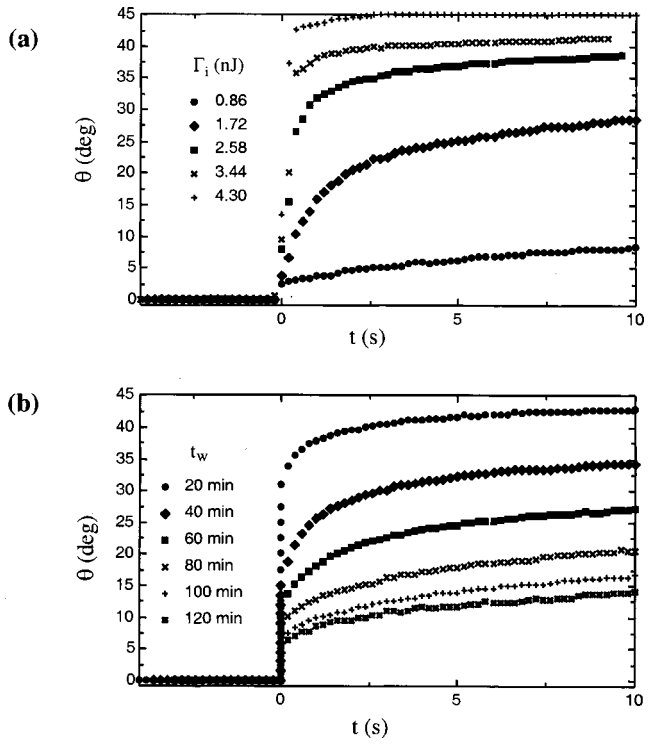

FIG. 9. Angle of the needle submitted to an oblique magnetic field ($\beta=45°$), as a function of time for (a) different initial torques at $t_w=20$ min (b) different aging times at $\Gamma_i=2.56$ nJ.

$\eta \approx F^{-\delta}$ with an exponent $\delta=(2.0\pm0.2)$ independent of the aging time.

E. Investigation of thixotropy using the rotating needle

We now investigate the mechanical behavior of the Laponite suspension with a different geometry of the mechanical perturbation, by using a ferromagnetic needle rotating in the fluid. The ferromagnetic needle is placed inside the fluid at $t=0$. At $t=t_w$, it is submitted to an external magnetic field. The initial angle between the field and the needle axis is 45°. Again, the rotation of the needle towards the magnetic field may be decomposed into three stages: first, an elastic regime in which the needle turns instantaneously in the fluid; then a transient regime and finally a slow relaxation towards equilibrium (see Fig. 9).

There is no analytical solution for the needle turning angle as a function of time in this case because the applied stress changes during the needle rotation. In addition, all the viscoelastic parameters of the fluid vary because of shear-thinning effect. Therefore, only the initial regime of the needle relaxation at $t'=0$ can be analyzed. At $t'=0^+$, just after the needle has turned instantaneously from an angle θ_0, the magnetic torque $\Gamma_+=\Gamma_0 \sin(45-\theta_0)$ applied to the needle equilibrates with the elastic torque exerted by the fluid to the needle. Figure 10(a) shows the variation of the fluid elastic constant C determined by the measurement of θ_0 using Eq. (11b) versus Γ_+. One notices that C is not a monotonic function of Γ_+. Therefore the linear analysis is, in the case of the rotating needle, unlikely to produce a proper estimation of the elastic constant of Laponite.

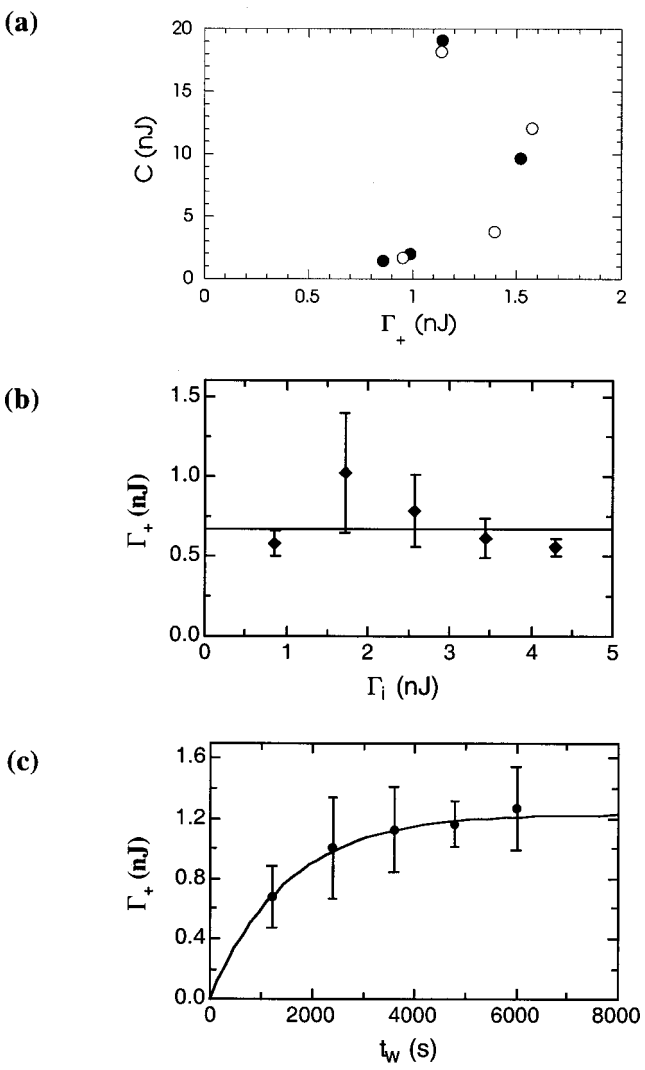

FIG. 10. (a) Variation of the Laponite linear elastic constant C obtained from Eq. (10a) as a function of the amplitude of the torque Γ_+ applied to the needle at $t'=0^+$, just after the instantaneous elastic angle step. Full circles, $t_w=60$ min; empty circles, $t_w=100$ min. The variation of C vs Γ_0 is erratic. Therefore, a linear model is not applicable to describe the rotation of the needle in the Laponite suspension. (b) Value of the torque Γ_+ just after the angle step, as a function of the initial torque Γ_i. The horizontal line represents the mean value (0.67 nJ here). The aging time is 20 min. (c) Evolution of the dynamical threshold value of the torque Γ_+ with the aging time t_w. The error bars represent the estimated standard error of the measurements for different initial torques. The plain curve represents an exponential relaxation function with a time constant of 1500 s and a saturation value of 1.23 nJ.

However, one notices that Γ_+ has no marked dependence on the initially applied torque [see Fig. 10(b)]. Over a wide range for Γ_i, the torque Γ_+ is constant within error. It seems that Laponite behaves as a dynamical yield stress fluid: when the stress is too large, the fluid ruptures under the stress and the needle turns instantaneously on the time scale of the observation, until the stress decreases to a threshold value. This threshold value is a nonlinear characteristic of the fluid. Persello *et al.* [43] have noticed a similar behavior in concen-

trated colloidal aqueous silica dispersions.[4] It is believed that when the stress is very intense the structure of the fluid is altered; the fluid then behaves as a brittle material, and intense shear localizes in fractures.

Plotting the dynamical yield stress as a function of the aging time [Fig. 10(c)], one notices a possible exponential relaxation behavior with a time constant of 25 min (1500 s). There is roughly a factor 2 difference with the aging time constant of the viscoelastic moduli, which is the same order of magnitude.

V. DISCUSSION

A. Validation of the local probes, and applications

In this paper, the rheology of viscoelastic complex fluids has been probed at a local but nevertheless macroscopic scale, using two different geometries for the perturbation. First, the translation of a magnetic bead inserted in the bulk of the material and submitted to a homogeneous controlled magnetic force has been used to determine the viscoelastic moduli of a Maxwellian micellar solution of surfactant. The values obtained are identical to within a few percent to those found using a traditional Couette rheometer, which validates the method. An interesting application of this local probe, based on the fact that the viscoelastic moduli are measured in the direction of the applied force, would be the investigation of the rheology of anisotropic fluids, such as the surfactant solution presented in Sec. III in the shear-banded regime (high applied stress).

The second technique is based on the rotation of a magnetic needle inside the fluid, under the influence of a controlled magnetic torque. Having extended the Maxwell model to the description of this geometry of perturbation, the viscoelastic moduli of the Maxwellian fluid have been measured via the analysis of relaxation of the needle orientation towards the direction of the applied magnetic field. Again, this method has been validated by the comparison with the results obtained using standard rheometric measurements. A further application of the rotating magnetic needle is based on the fact that in this geometry, the elastic and viscous torques applied to the needle both scale as the needle volume, as well as the magnetic torque. Therefore, at mechanical equilibrium, the equation of motion of the needle does not depend on the needle volume, contrary to the case of the translating bead. It should thus be possible to continuously vary the size of the magnetic probe from a millimetric to a nanoscopic scale. In the case of complex fluids, which are structured at many different length scales, the rheological response of the fluid is expected to change when the probe reaches a size comparable to a characteristic length scale of the fluid. This tool can thus be used to explore the link between rheology and structure in complex fluids. Applying an oscillating stress will also allow to perform a complete rheological study, probing all the pertinent lengths and time scales of the analyzed material.

B. Application to the rheology of a Laponite suspension

Having validated the experimental methodology, the local probes have been used to investigate aging, shear thinning, and thixotropy of the isotropic pasty phase of a Laponite colloidal suspension, whose rheology is still poorly understood. We have found that the characteristic rheological relaxation time τ of the fluid grows exponentially with the age of the system t_w. This result confirms recent independent measurements performed on Laponite suspension using dynamic light scattering (DLS) [35]. Both experiments have been performed in the early stage of aging, when the typical relaxation time of the system is small compared to the system age, $\tau \ll t_w$ ($\tau/t_w \approx 10^{-2}$ in the experiments presented in this paper). In a later stage of aging, when τ is of the order of t_w, a power-law scaling of τ versus t_w is generally observed, in Laponite suspensions [11] and in many other physical systems [9,36,38,42]. The good agreement between our results and the results obtained using DLS [35] is instructive, as relaxation times determined using DLS or rheological measurements are of a different nature. DLS allows to determine a microscopic relaxation time, which is the time for the positions of the colloidal Laponite particles to decorrelate. Rheology measures a macroscopic characteristic time, defined as the ratio between the fluid viscous and elastic modulus. In aging systems, which are out of equilibrium, no link exists *a priori* between the microscopic fluctuations and the fluid viscosity, although such a relation is experimentally observed. More experiments, coupling DLS and rheological measurements, are needed to explore this link.

Varying the applied stress, we have found that the variation of the viscosity η of the pasty phase of Laponite *versus* the applied force F is compatible with a power law: $\eta \approx F^{-\delta}$ with an exponent $\delta = (2.0 \pm 0.2)$ independent of the system age. This result can be compared to the measurement of Bonn *et al.* [40] performed on Laponite suspension using a Couette rheometer. Varying the shear rate $\dot{\varepsilon}$ of the shearing plate, the authors have found that the fluid viscosity η scales as a power law with the shear rate: $\eta \approx \dot{\varepsilon}^{-\nu}$ with $\nu = (0.66 \pm 0.02)$. Assuming that the force is proportional to $\eta\,\dot{\varepsilon}$ in the viscous regime, this measurement gives $\delta = \nu/(1-\nu) = (1.9 \pm 0.1)$, which is in good agreement with our measurements. This similarity is, however, surprising as the experimental procedure in both methods is different. Bonn *et al.* have performed measurements in the stationary regime, reached after shearing the fluid for several hours in a Couette rheometer. In our experiments, the viscosity is measured a few seconds after the force is applied to the magnetic bead, and the bead explores a region that has not been previously sheared. The similarity between both measurements suggests that the aging and shear-thinning behavior of Laponite could be independent, the viscosity of the suspension being a product of a function of t_w times a function of the applied force or shear rate.

Finally, using the magnetic needle rotating inside the Laponite suspension, we have investigated a nonlinear re-

[4] In the case of the concentrated silica colloid, the volume fraction was over 0.25. It is known that Laponite dispersion exhibit the same generic behavior as silica dispersion, only at much lower volume fractions [7].

gime, in which the stress applied to the needle instantaneously relaxes to a fixed value, independent of the initial applied magnetic torque. This behavior is compatible with the fracturation of the pasty phase, which is responsible of the thixotropy of colloidal suspensions. The applied threshold torque above which the fracture regime appears increases with the age of the suspension, with a characteristic time which is of the same order of magnitude as the increasing time of the suspension rheological time.

To unify the different regimes investigated with the translating bead and with the rotating needle, a proper estimation of the stress applied to the fluid is needed. In the case of the translating bead, the applied stress as a function of the applied force amplitude can be written as: $\sigma \cong F_0/(4\pi R^2)$, where R is the radius of the bead. For the range of the used force amplitudes, between 18 and 37 μN, the stress σ applied to the bead ranges between 5 and 10 Pa. The stress applied at the tip of the rotating needle can be estimated as $\sigma \cong \Gamma_i/(12\pi L^3)$, where L is the length of the needle. As Γ_i varies between 0.6 and 3.9 nJ during experiments, this corresponds to a stress σ applied to the tip of the needle between 16 and 95 Pa. However, the viscoelastic internal stress is not homogeneous at the surface of the probe, and these considerations only give an order of magnitude estimate of the applied stress during the experiment. We can still conclude that the maximum stress applied at the tip of the rotating needle is in average higher than the stress applied to the translating bead. This is compatible with the fact that the bead explores the pasty phase of the Laponite suspension investigated, whereas the needle explores the transition from the pasty phase to the liquid phase, which occurs when the stress increases.

VI. CONCLUSION

In this paper, we have introduced an experimental method to locally investigate the rheology of complex fluids. A magnetic probe, inserted in the bulk of the fluid, is submitted to a controlled external magnetic stress. The viscoelastic moduli of the fluid are deduced from the analysis of the motion of the probe in the fluid. This experimental methodology has first been validated using a well-known fluid having a linear Maxwellian rheological behavior. Then, the rheology of a Laponite colloidal suspension has been investigated. We have obtained the following results.

(1) *Aging*. The characteristic rheological time of the suspension increases exponentially with the age of the suspension. The experiments have been performed in the early stage of aging, where the characteristic rheological time is small compared to the system age.

(2) *Shear thinning*. The viscosity of the suspension decreases when the applied stress increases. This decrease is compatible with a power law: $\eta \approx \sigma^{-\delta}$ with $\delta = (2.0 \pm 0.2)$ independent of the system age.

(3) *Thixotropy*. Above a threshold applied stress, the rotating needle shows a regime which is compatible with a fracture regime in the fluid, and could be the beginning of the transition from the viscoelastic phase towards a liquid phase. This yield stress is an increasing function of the suspension age.

The experimental methods presented in this paper are promising for future investigation of complex fluids. The translating bead can be used to determine the viscoelastic moduli of anisotropic fluids. The rotating needle will be used to probe, by the means of rheology, all the pertinent length and time scales of a complex fluid, by varying the frequency of the applied stress, and the size of the probe from a millimetric to a nanoscopic scale.

ACKNOWLEDGMENTS

We acknowledge F. Cousin for his help during the preparation of the Laponite suspensions and enlightening discussions. Thanks are due to E. Terentjev, S. Clarke, B. Abou, and D. Bonn for fruitful criticisms.

[1] R. G. Larson, *The Structure and Rheology of Complex Fluids* (Oxford University Press, New York, 1999).
[2] S. M. Fielding, P. Sollich, and M. E. Cates, J. Rheol. **44**, 323 (2000).
[3] G. Porte, J.-F. Berret, and J. L. Harden, J. Phys. France **7**, 459 (1997).
[4] H. A. Barnes, J. Non-Newtonian Fluid Mech. **70**, 1 (1997).
[5] J. D. Ferry, *Viscoelastic Properties of Polymers* (Wiley, New York, 1980).
[6] P. Olmsted and C.-Y. D. Lu, Phys. Rev. E **56**, 55 (1997).
[7] T. G. Mason and D. A. Weitz, Phys. Rev. Lett. **74**, 1250 (1995); T. G. Mason, H. Gang, and D. A. Weitz, J. Mol. Struct. **383**, 81 (1996).
[8] D. Bonn, H. Tanaka, G. Wegdam, H. Kellay, and J. Meunier, Europhys. Lett. **45**, 52 (1998).
[9] L. Cipelletti, S. Manley, R. C. Ball, and D. A. Weitz, Phys. Rev. Lett. **84**, 2275 (2000).
[10] R. Hölher, S. Cohen-Addad, and H. Hoballah, Phys. Rev. E **79**, 1154 (1997).
[11] A. Knaebel, M. Bellour, J.-P. Munch, V. Viasnoff, F. Lequeux, and J. L. Harden, Europhys. Lett. **52**, 73 (2000).
[12] J. C. Crocker, M. T. Valentine, E. R. Weeks, T. Gisler, P. D. Kaplan, A. G. Yoth, and D. A. Weitz, Phys. Rev. Lett. **85**, 888 (2000).
[13] J.-L. Barat and L. Berthier, Phys. Rev. E **63**, 012503 (2000).
[14] F. Ziemann, J. Rädler, and E. Sackmann, Biophys. J. **66**, 2210 (1994).
[15] F. Amblar, B. Yurke, A. Pargellis, and S. Leibler, Rev. Sci. Instrum. **67**, 818 (1996).
[16] F. Amblar, A. C. Maggs, B. Yurke, A. Pargellis, and S. Leibler, Phys. Rev. Lett. **77**, 4470 (1996).
[17] A. R. Bausch, W. Möller, and E. Sackmann, Biophys. J. **76**, 573 (1999).
[18] J.-C. Bacri, J. Dumas, D. Gorse, R. Perzynski, and D. Salin, J.

Phys. (France) Lett. **46**, 1199 (1985).
[19] J.-C. Bacri, D. Salin, R. Perzynski, V. Cabuil, and R. Massart, J. Magn. Magn. Mater. **62**, 36 (1986).
[20] M. E. Cates and S. J. Candau, J. Phys.: Condens. Matter **2**, 6869 (1990).
[21] M. E. Cates, Macromolecules **20**, 2289 (1987).
[22] Ch. W. Macosko, *Rheology: Principles, Measurements and Applications* (Wiley-VCH, New York, 1994).
[23] L. Landau and E. Lifschitz, *Theory of Elasticity*, 3rd ed. (Pergamon, Oxford, 1986).
[24] V. M. Laurent, S. Hénon, E. Planus, E. Planus, R. Fodil, M. Bellaud, D. Isabey, and F. Gallet, J. Biomech. Eng. (to be published).
[25] M. Doi and S. F. Edwards, *The Theory of Polymer Dynamics* (Clarendon, Oxford, 1988).
[26] M. Kroon, W. L. Vos, and G. H. Wegdam, Phys. Rev. E **57**, 1962 (1998).
[27] F. Cousin, V. Cabuil, and P. Levitz, Langmuir **18**, 1466 (2002).
[28] A. Mourchid, E. Lecolier, H. Van Damme, and P. Levitz, Langmuir **14**, 4718 (1998).
[29] F. Pignon, J.-M. Piau, and A. Magnin, Phys. Rev. Lett. **76**, 4857 (1996).
[30] M. Kroon, G. H. Wegdam, and R. Sprik, Phys. Rev. E **54**, 6541 (1996).
[31] D. Bonn, H. Kellay, H. Tanaka, G. Wegdam, and J. Meunier, Langmuir **15**, 7534 (1999).
[32] A. Mourchid and P. Levitz, Phys. Rev. E **57**, R4887 (1998).
[33] F. Cousin, Ph.D. thesis, Université Pierre et Marie Curie, 2000.
[34] E. Trizac and J.-P. Hansen, Phys. Rev. E **56**, 3137 (1997).
[35] B. Abou, D. Bonn, and J. Meunier, Phys. Rev. E **64**, 021510 (2001).
[36] M. Cloitre, R. Borrega, and L. Leibler, Phys. Rev. Lett. **85**, 4819 (2000).
[37] C. Derec, A. Ajdari, and F. Lequeux, Eur. Phys. J. E **4**, 355 (2001).
[38] C. Derec, A. Ajdari, G. Ducouret, and F. Lequeux, C. R. Acad. Sci. Paris, Série IV **1**, 1115 (2000).
[39] D. Bonn, S. Tanase, B. Abou, H. Tanaka, and J. Meunier (unpublished).
[40] D. Bonn, P. Coussot, H. T. Huyn, F. Bertrand, and G. Debrégeas (unpublished).
[41] D. W. Thompson and J. T. Butterworth, J. Colloid Interface Sci. **151**, 236 (1992).
[42] L. C. E. Struik, *Physical Aging in Amorphous Polymers and Other Materials* (Elsevier, Houston, 1977).
[43] L. Persello, A. Magnin, J. Chang, J. M. Piau, and B. Cabane, J. Rheol. **38**, 1845 (1994).